THE JOURNAL OF PHYSICAL CHEMISTRY Letters

Letter

pubs.acs.org/JPCL

Correlated Fluctuations and Intraband Dynamics of J-Aggregates Revealed by Combination of 2DES Schemes

Luca Bolzonello,[†] Francesca Fassioli,*[,‡] and Elisabetta Collini*[,†]

[†]Department of Chemical Sciences, University of Padova, Via Marzolo 1, Padova 35131, Italy

[‡]Department of Physics, University of Trieste, Strada Costiera 11, Trieste 34151, Italy

Supporting Information

ABSTRACT: The intraband exciton dynamics of molecular aggregates is a crucial initial step to determine the possibly coherent nature of energy transfer and its implications for the ensuing interband relaxation pathways in strongly coupled excitonic systems. In this work, we fully characterize the intraband dynamics in linear J-aggregates of porphyrins, good model systems for multichromophoric assemblies in biological antenna complexes. Using different 2D electronic spectroscopy schemes together with Raman spectroscopy and theoretical modeling, we provide a full characterization of the inner structure of the main one-exciton band of the porphyrin aggregates. We find that the redistribution of population within the band occurs with a characteristic time of 280 fs and dominates the modulation of an electronic coherence. While we do not find that the coupling to vibrations significantly affects the dynamics of excitonic coherence, our results suggest that exciton fluctuations are nevertheless highly correlated.

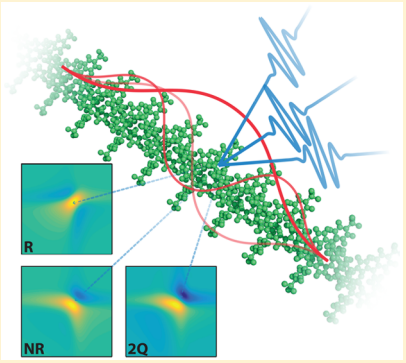

Despite being the object of thorough theoretical and experimental studies for more than 60 years,[1−3] J-aggregates continue to arouse considerable interest.[4−7] Such interest is mainly due to the collective nature of their optical excitations, known as excitons, endowed with unique linear and nonlinear optical responses.[7,3−10] The attention on these systems has recently been renewed after the discovery that light-harvesting complexes in natural photosynthetic systems are governed by principles very similar to those holding in aggregates of artificial dyes.[11] It has been recognized that excitons play a fundamental role in the mechanism of electronic energy transfer, which can notably include quantum coherent dynamics, in various synthetic nanoscale and biological systems.[12−16] In light of the possible role of quantum coherence in exciton transfer, the attention is currently focused on the characterization of transport properties of excitonic systems and how they are affected by the coupling with vibrations and the environment.[5,17−22] An important aspect in this regard, still not fully investigated, is intraband dynamics (i.e., the dynamics within states building the optically active one-exciton band) in J-aggregates, foregoing the more characterized interband dynamics.

In this work, different 2D electronic spectroscopy (2DES) schemes have been applied together with Raman spectroscopy and theoretical modeling to fully characterize the intraband exciton dynamics in porphyrin J-aggregates at room temperature, with particular attention to the effects of the coupling between electronic and vibrational degrees of freedom.

Aggregates of porphyrins, in particular of the diacid form of the water-soluble tetra-(*p*-sulphonato)-phenyl-porphyrin (H_2TPPS) (Figure 1a), are particularly meaningful because they have been often proposed as model systems for chlorosomes and LH2 complexes.[23,24] The aggregation properties of H_2TPPS are well known, and a significant number of works have already been devoted to clarify the aggregation conditions, the aggregate geometry and structure, and the photophysical and dynamical properties in both monomeric and aggregated form. The appearance of new blue- or red-shifted bands in the absorption spectra is a typical signature of aggregate formation (Figure 1b).[6,7,3,25−30] The optical properties of H_2TPPS aggregates are typically described using an ideal model of a linear homogeneous aggregate of N monomers with nearest-neighbor coupling only.[7] In this model the expression of eigenstates and eigenenergies can be calculated exactly. The one-exciton band is formed by N eigenstates $|k\rangle$, characterized by a single quantum number k and an energy $E_k = E + 2J\cos(\pi k/(N+1))$, where E is the energy of the excited state of the monomer and $J < 0$ is the electronic coupling.[6,3] The state with $k = 1$ ($|1\rangle$) collects the majority of the oscillator strength, and the rest is distributed among all of the odd k states with a decreasing relevance as k increases, such that the linear optical properties can be justified considering only the first two optically bright states $|1\rangle$ and $|3\rangle$. The description of nonlinear optical properties requires us to invoke also the two-exciton band, which is formed by states $|k, k'\rangle$ ($k \neq k'$) with energies related to the one-exciton energies by $E_{k,k'} = E_k + E'_k$.[31] Exciton binding interactions leading to biexciton formation can be neglected in these systems.[28,32]

Received: October 19, 2016
Accepted: November 22, 2016
Published: November 22, 2016

DOI: 10.1021/acs.jpclett.6b02433
J. Phys. Chem. Lett. 2016, 7, 4996−5001

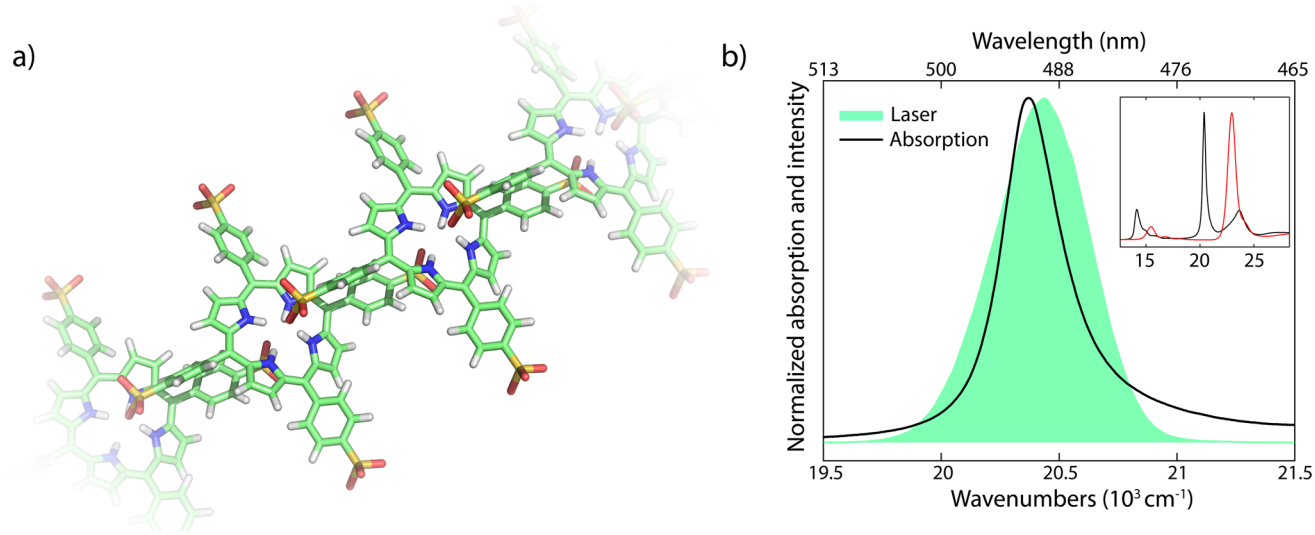

Figure 1. (a) Schematic of the linear self-assembled geometry of H_2TPPS aggregates. (b) Steady-state absorption spectrum of the H_2TPPS aggregate in water solution in the J_B band region (black) and experimental spectrum of the exciting laser pulse used in 2D spectroscopy (green shadowed area). The band is generated by the interaction of dipole moments oriented parallel along the linear chain (head-to-tail configuration).[33] The inset compares the absorption spectra in the whole visible range for the monomer (red) and the aggregate (black), where new excitonic bands are detected at ~23 700 cm^{-1} (H_B), 20 400 cm^{-1} (J_B), and 14 200 cm^{-1} (J_Q).[3,25,33] The J_B band in the aggregate is shifted by ~2660 cm^{-1} to the red with respect to that of the monomer, so that $E_1 - E = 2J\cos(\pi/(N+1)) \approx -2660$ cm^{-1}.

In this work we focus on the so-called J_B band[27,33] located at 20 380 cm^{-1} (~490 nm), which is characterized by the higher excitonic coupling. The exciting laser band in 2D experiments has thus been tuned to cover the above-mentioned band (Figure 1b). Details of 2D spectroscopy and the physical meaning of 2D signals can be found in refs 34 and 35. The optical setup and data analysis techniques specifically employed in this work are described in the SI.

Figure 2a shows two examples of 2D maps measured in the rephasing (R) and nonrephasing (NR) schemes, recorded at waiting time $t_2 = 0$ fs. t_2 is the time delay between the second pump and the probe pulses, during which the population and coherence dynamics take place.[35] For all times t_2 investigated, the R signal is dominated by a positive diagonal peak elongated along the diagonal direction, while the NR map is dominated by a positive diagonal peak elongated in the antidiagonal direction, both attributed to ground-state bleaching and stimulated emission of the J_B transition. The upper and lower off-diagonal (diagonal) negative features in R (NR) spectra are the result of the typical dispersion lineshapes. The possible contribution of an excited-state absorption from one-exciton to the two-exciton states can be invoked to explain the slight asymmetry of the upper negative peak, being more intense than the lower one, although the process cannot be fully captured in the analyzed spectral range. (see SI Figure S1)

The absence of distinct features in the R and NR 2D maps does not allow the clear characterization of the internal structure of the J_B band. To gain more insight, 2D experiments have been repeated in the so-called "double-quantum" scheme (2Q2D), reported in the last column of Figure 2a. 2Q2D is able to capture the transition toward two-exciton states in the absence of all of the other superimposed R and NR contributions. In a 2Q2D experiment, a nonnegligible signal is detected only if the system is at least a three-level system.[35,40−43] The sequence of pulses is such that the first two pulses generate a double-quantum coherence between the ground (g) and a two-exciton state (f), whose phase oscillates during t_2 at the frequency of the g–f energy gap, close to twice the frequency of the ground and single exciton (g–e) gap, in resonance with the exciting pulse. The third excitation pulse then returns the system to a one-quantum coherence (g–e or e–f), and the signal is emitted. Differently from R and NR 2D maps, a 2Q2D map is obtained varying t_2 for fixed values of t_1, and thus it reports the signal as a function of ω_2 and ω_3 (see the SI). The 2Q2D technique is particularly suited in the case of J-aggregates because it allows determining the position of the two-exciton states with respect to the one-exciton transitions. Moreover, because the two-exciton state energies are related to the one-exciton state energies, a 2Q2D experiment can provide information also on the one-exciton band structure. In the absence of line-broadening effects the distance between the positive and the negative peaks along the ω_3 axis $\Delta_{\omega 3}$ in a 2Q2D map corresponds to the difference between the two-exciton to one-exciton energy gap and the one-exciton to ground-state energy gap, that is, $\Delta_{\omega 3} = (E_f - E_e) - (E_e - E_g)$. Homogeneous broadening results in a slight increase in this distance as well a shift of the peaks along the ω_2 axis.[41] For linear J-aggregates, the selection rules state that the transitions with the highest oscillator strength are $|0\rangle \rightarrow |1\rangle$ and $|1\rangle \rightarrow |1, 2\rangle$;[11,44] therefore, we can identify $e = |1\rangle$ and $f = |1, 2\rangle$ and the energy difference $\Delta_{\omega 3}$ can be related to the $k = 2$ and $k = 1$ exciton gap, $\Delta_{\omega 3} \gtrsim (E_f - E_e) - (E_e - E_g) = E_2 - E_1$. The estimation of the $E_2 - E_1$ gap from 2Q2D measures ($\Delta_{\omega 3} \approx 180$ cm^{-1}, Figure 2a) and the estimation of the $E_1 - E$ gap from linear absorption measures (Figure 1), allow extrapolating the values of J and N that best reproduce experimental data using the expression of exciton energies. A $k = 2$ and $k = 1$ exciton gap in the range of $E_2 - E_1 \approx 160-200$ cm^{-1} leads to $-J \approx 1170-1400$ cm^{-1} and $N \approx 12-14$. Using the same expression, these values have been then used to estimate the exciton gap between the states $|1\rangle$ and $|3\rangle$, $E_3 - E_1 \approx 420-520$ cm^{-1} (see the SI).

This estimated energy gap is also consistent with the analysis of the time dependence of the R and NR 2D maps. The dynamic evolution of such 2D maps along t_2 has been studied

DOI: 10.1021/acs.jpclett.6b02433
J. Phys. Chem. Lett. 2016, 7, 4996−5001

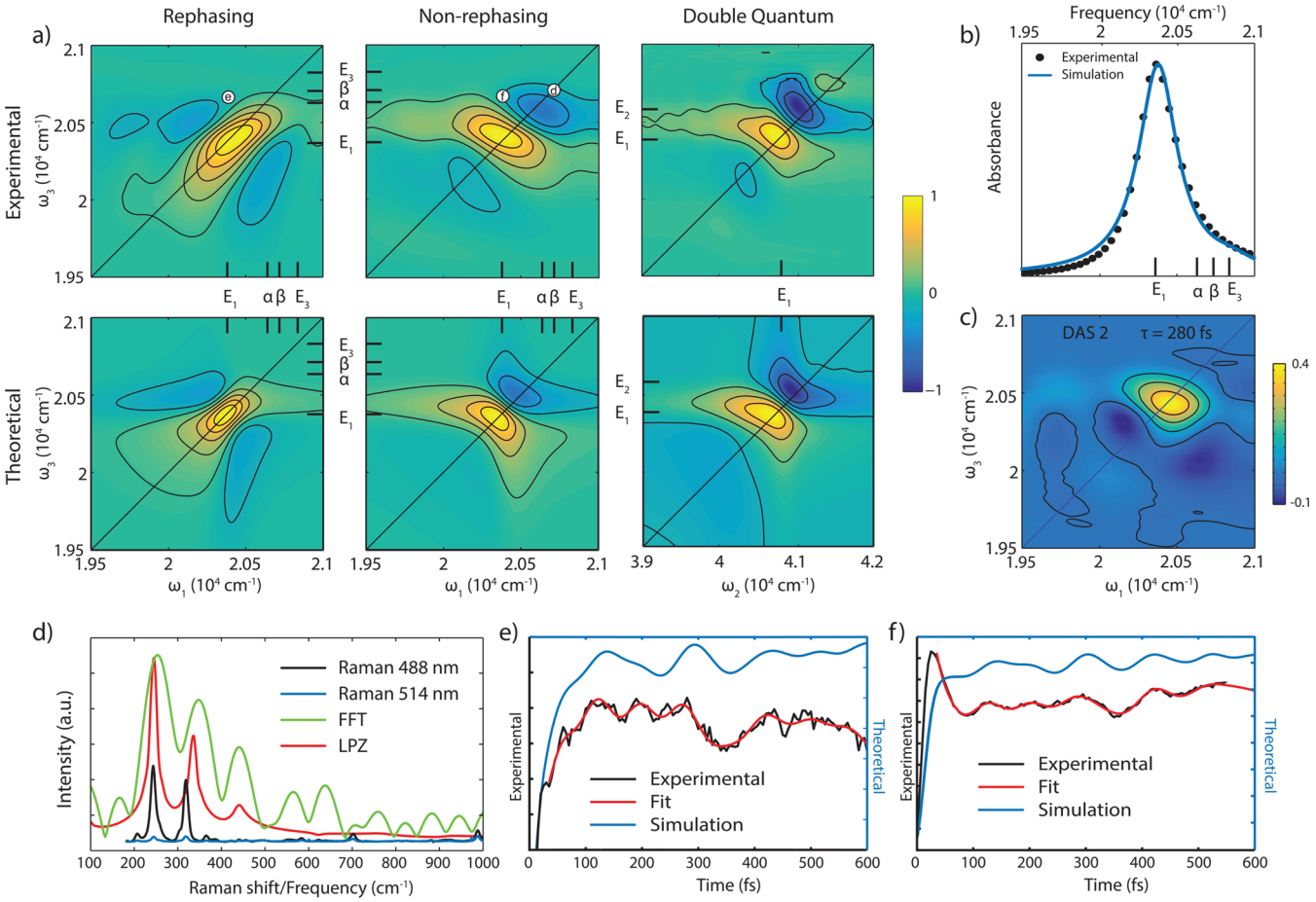

Figure 2. (a) Examples of experimental (upper line) and simulated (lower line) 2D maps obtained in the rephasing (R), non rephasing (NR), and double-quantum (2Q) configurations for H_2TPPS aggregates in solution at room temperature. The R and NR maps report the real part of the signal at $t_2 = 0$ fs. The 2Q maps refer to $t_1 = 0$. All of the maps are normalized to their maximum. The energies of relevant states and the coordinates where the traces shown in panels d–f are extracted are also pinpointed in the maps. (b) Simulation of the absorption spectrum. The parameters used to simulate linear and 2D response are reported in the SI. (c) Decay-associated spectrum (DAS)[36] of the purely absorptive (R+NR) maps, showing the amplitude distribution of the 280 fs time constant. A positive (negative) amplitude is recorded, where the signal is decaying (rising). (d) Comparison between beating modes in Raman and 2D spectra. Fourier transform (green) and linear prediction z-transform LPZ[37−39] (red) of the oscillating part of the NR signal extracted at coordinates where all three main oscillating components are expected to contribute. Resonant (black) and nonresonant (blue) Raman spectra. (e,f) Comparison of the experimental and theoretical decay traces as a function of t_2 in R (e) and NR (f) signals extracted at relevant coordinates $(\omega_1, \omega_3) \approx (E_1, E_1 + \omega_\alpha)$.

with a recently proposed global analysis methodology able to simultaneously extract coherence and population dynamics of R and NR contributions.[36] The results of this analysis are reported in Table 1.

Table 1. Results of the Global Multiexponential Fit of the 2D Maps (see SI and ref 36)[a]

component[b]	DAS 1	DAS 2	CAS 1	CAS 2	CAS 3
time constant (ps)	>1	0.28	>1	>1	0.265
frequency (cm^{-1})			258	334	445

[a]Standard errors of the fit are in the order of 1% for frequencies and 15% for time constants. [b]DAS, decay-associated spectrum; CAS, coherence-associated spectrum as defined in ref 36.

The population dynamics of the purely absorptive signal is dominated by two time constants, whose amplitude distributions in the 2D maps are shown in the form of decay-associated spectra[36] (DAS). Together with a long time constant (>1 ps) describing the overall decay of the maps, the dynamics in the investigated time window is characterized by a time constant of 280 fs. The amplitude distribution of this time constant (DAS in Figure 2c) shows a positive peak (i.e., signal is decaying) on the upper diagonal, whereas negative peaks (i.e., signal is raising) are present on the lower diagonal and off-diagonal positions. This witnesses a transfer of signal amplitude from higher to lower energy states with a 280 fs time constant. Other ultrafast dynamic phenomena typically characterized by similar time scales, such as spectral diffusion, would have presented significantly different amplitude distributions.[36] We therefore suggest that this time constant is associated with a population redistribution within the J_B band, from states at higher energy to states at the bottom of the band.

The evolution of the 2D signal also shows the presence of oscillations, typical signatures of the coherent evolution of the quantum superpositions prepared by the exciting laser. The same global analysis allows identifying three frequency components contributing to the overall 2D map beating: 258, 334, and 445 cm^{-1} (Figure 2d).

The first two components contribute in both R and NR maps with damping times longer than the time window investigated (>1 ps) and can be interpreted as vibrational coherences.

DOI: 10.1021/acs.jpclett.6b02433
J. Phys. Chem. Lett. 2016, 7, 4996−5001

This assignment is also endorsed by the results of off- and on-resonance Raman measurements (Figure 2d), showing indeed a strong enhancement of two low-frequency vibrational modes at 246 and 319 cm^{-1}.

The third frequency component does not match any relevant vibrational mode but is very close to the excitonic gap $E_1 - E_3$ estimated through the combined 2Q2D measures and model analysis. Differently from the other two components, it is damped within the first 265 fs after photoexcitation.

This evidence suggests that the 445 cm^{-1} oscillation has an electronic origin and corresponds to the evolution of the coherent superposition between the states $|1\rangle$ and $|3\rangle$, initially prepared by the laser pulse. Note that the dephasing time of this coherence is very similar to the relaxation time discussed above.

To support the interpretation of our data, the experimental optical responses have been simulated using a minimal model for the excitations and vibrations in the aggregate that can describe the most prominent features of the spectra. Given that most of the oscillator strength is on the $|1\rangle$ and to a lower degree on $|3\rangle$ exciton transition, we consider a four-level electronic system, consisting of the ground state ($|0\rangle$), the two $k = 1$ and $k = 3$ one-exciton states, and the lowest two-exciton state $k, k' = 1, 2$ ($|1,2\rangle$). The vibronic coupling in this minimal model is included by considering the coupling of the electronic states to two effective vibrational modes. The total Hamiltonian of the system is given by $H_s = H_{el} + H_{el,vib} + H_{vib}$ with the electronic Hamiltonian given by $H_{el} = E_1|1\rangle\langle 1| + E_3|3\rangle\langle 3| + E_{12}|1, 2\rangle\langle 1, 2|$ and the vibrational Hamiltonian $H_{vib} = \hbar\omega_\alpha a_\alpha^\dagger a_\alpha + \hbar\omega_\beta a_\beta^\dagger a_\beta$, where the operators $a_{\alpha(\beta)}^\dagger$ and $a_{\alpha(\beta)}$ denote the creation and annihilation operators of phonon modes, respectively, and $\omega_{\alpha(\beta)}$ is the vibrational frequency. Finally, for the electron-vibrational coupling we find that an interaction of the type $H_{el,vib} = \sum_{i=\alpha,\beta} g_i(a_i^\dagger + a_i)(|1\rangle\langle 3| + |3\rangle\langle 1|)$, which takes into account the coupling of the one-exciton states by the vibrations but neglects the displacement on each excited state, best describes the experimental results. This can be justified in the light of the weak vibronic coupling, as detailed in the SI.

We include decoherence, leading to homogeneous broadening, by coupling the system to a Markovian environment that induces exponential decay of electronic coherence at rates Γ_{ij} but not population transfer (for details, see the SI). In particular, the electronic decoherence rates Γ_{0k} ($k = 1, 3$) describe the decay rate of the coherence between the electronic ground state and the one-exciton state k, while Γ_{13} represents the decay rate of the coherent superposition of the two one-exciton states and in general includes correlated fluctuation effects. Static disorder has been considered negligible in our calculations. This assumption, typically verified in the case of strongly coupled J-aggregates,[45] is also justified by the round shape of the absorptive spectra (Figure S5 of the SI).[46]

This model has been used to simulate the absorption spectrum (Figure 2 b) and all of the 2D experiments (R, NR, and 2Q schemes). All of the parameters are given in the SI. In the simulation of the nonlinear experiments, the molecular response to laser excitation is described in the framework of the response function formalism,[47] and the finite pulse duration of the exciting pulses has been considered so that possible pulse overlap effects have been accounted for (see the SI).

Figure 2a shows the simulated 2D maps at $t_2 = 0$. The position and relative strengths of the positive and negative peaks are in good agreement with the experimental data. The broadening of the positive peaks is slightly narrower in our calculations. Because we reproduce the absorption width (Figure 2b) it is possible that this difference is due to other experimental pulse effects that have not been captured in the simulations. Also, the dynamic behavior of the 2D maps along t_2 could be properly reproduced, as shown in Figure 2e,f.

The values of the coupling constants g_i optimizing the simulations ($g_\alpha = 0.24\omega_\alpha$ and $g_\beta = 0.2\omega_\beta$) suggest that the two vibrations are only weakly coupled to the electronic transition giving rise to the J_B band. We found that the vibronic coupling does not alter in a relevant way the energies and the properties of the excited states and the aggregate. In particular, this degree of vibronic coupling does not significantly mix different electronic states, and the energies of the strongest vibronic transitions are relatively close to those of the simplistic linear chain electronic system such that the insight gained from the purely electronic chain regarding the energies of the single-exciton and two-exciton states holds.

It is also interesting to highlight the values found for the decoherence rates: $\Gamma_{01} = 26\ ps^{-1}$, $\Gamma_{03} = 40\ ps^{-1}$, and $\Gamma_{13} = (0.265\ ps)^{-1} = 3.8\ ps^{-1}$. The dephasing rate Γ_{13} resulted in being much slower than what was predicted for uncorrelated dephasing:[5] $\Gamma_{13} \ll \Gamma_{01} + \Gamma_{03} = 66\ ps^{-1}$ (see the SI). This suggests that correlated fluctuations are a fundamental intraband mechanism in such strongly coupled aggregates. Correlated dephasing mechanisms can be due to excitons sharing the same pigments even when the environment-induced fluctuations at each molecule are uncorrelated (local baths) as well as molecules experiencing correlated fluctuations (shared bath).[5,48,49] Both processes are equally likely in the case of intraband relaxation processes, where the relaxation involves one-exciton states described as a combination of the same molecular states with different symmetry.

In conclusion, the synergic use of several 2D techniques, including a double-quantum experiment, allowed a full characterization of the inner structure of the one-exciton J_B band of H_2TPPS aggregates, including a dark state ($k = 2$) not detectable with conventional techniques and two weakly coupled vibrational modes (Figure 3). The intraband dynamics of the most intense one-exciton band in the aggregates is characterized by an internal population relaxation toward the bottom of the band with a characteristic time of 280 fs, and it is modulated by the evolution of a coherent superposition of excitonic states dephasing on the same time scale. This time is considerably longer than what is expected only on the basis of spectral line-width considerations. The simulation of the experimental data with a theoretical model taking into account the possible coupling between vibrational modes and electronic transitions and the dephasing action of the environment lead to the conclusion that the long-living character of such electronic coherence cannot be explained with the mixing between vibrational and electronic degrees of freedom, as proposed for other multichromophoric systems.[5,50,51] This is expected in light of previous work suggesting that such mechanism requires the presence of vibrational modes having a frequency resonant with the electronic transition,[5,52] which is clearly not the case here where two weakly coupled low-frequency modes dominate the modulation of the optical response. The long dephasing time of the intraband electronic coherence captured in this work seems instead to be due to the presence of other environmentally induced correlated dephasing mechanisms. On the contrary, experimental data also suggest that the main dephasing mechanism is the population decay. The electronic coherence is indeed damped on a time scale corresponding to

DOI: 10.1021/acs.jpclett.6b02433
J. Phys. Chem. Lett. 2016, 7, 4996−5001

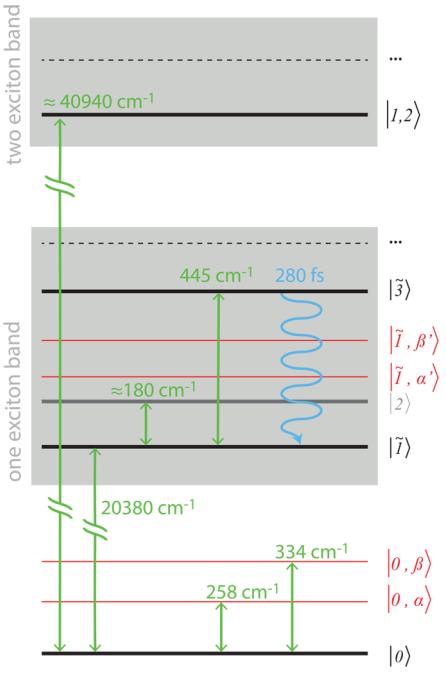

Figure 3. Model level scheme as determined by experiments and theoretical modeling. $|0\rangle$ is the ground state and $|0, \alpha(\beta)\rangle$ are the two main vibrational states on the ground electronic state. $|\tilde{k}\rangle$ indicates vibronic states in the one-exciton band with predominant k electronic character (black lines) and $|\tilde{k}, \alpha'(\beta')\rangle$ are vibronic states with predominant k electronic character and $\alpha(\beta)$ vibrational character (red lines). $|2\rangle$ is a dark state whose energy could be approximately determined only with 2Q2D experiments (gray line).

the relaxation of the population toward the state with the lowest energy. These findings represent an important piece of information in the debated issue of the possible relevance of correlated fluctuations[53] in energy and charge transport processes. The nature of such correlations and their influence on dynamics can indeed be crucial to begin to design environments that can be self-assembled to take advantage of these correlations as a mechanism to control energy and charge transport in fluctuating nanostructured environments. Furthermore, the characterization of the intraband dynamics is particularly important considering that other ensuing interband processes, including energy transfer, may involve an ultrafast energy equilibration as the initial step. It would be interesting to understand if this process has any effect on the overall energy-transfer rate, especially given the close resemblance of such aggregates with biological antennas.

■ ASSOCIATED CONTENT

Supporting Information

The Supporting Information is available free of charge on the ACS Publications website at DOI: 10.1021/acs.jpclett.6b02433.

Detailed theoretical modeling and methodologies for the simulations of 2D maps. Experimental methodologies and additional 2D maps. (PDF)

■ AUTHOR INFORMATION

Corresponding Authors

*E-mail: Francesca.Fassioli@ts.infn.it.
*E-mail: elisabetta.collini@unipd.it.

ORCID

Elisabetta Collini: 0000-0002-1019-9100

Notes

The authors declare no competing financial interest.

■ ACKNOWLEDGMENTS

This work is supported by the ERC Starting Grant QUENTRHEL (278560) and FP7 EU STREP project PAPETS (323901). F.F. kindly acknowledges financial support from the Marie Curie Individual Fellowships FP7-PEOPLE-2013-IEF project QUANTUM VIBES (629254).

■ REFERENCES

(1) Scheibe, G. Über die Veränderlichkeit der Absorptionsspektren in Lösungen und die Nebenvalenzen als ihre Ursache. *Angew. Chem.* **1937**, *50*, 212−219.
(2) Jelley, E. Molecular, Nematic and Crystal States of I: I-Diethyl−Cyanine Chloride. *Nature* **1937**, *139*, 631−631.
(3) Kobayashi, T. *J-Aggregates*; World Scientific, 1996; Vol. *1*.
(4) Sung, J.; Kim, P.; Fimmel, B.; Würthner, F.; Kim, D. Direct observation of ultrafast coherent exciton dynamics in helical π-stacks of self-assembled perylene bisimides. *Nat. Commun.* **2015**, *6*, 8646.
(5) Lim, J.; Paleček, D.; Caycedo-Soler, F.; Lincoln, C. N.; Prior, J.; von Berlepsch, H.; Huelga, S. F.; Plenio, M. B.; Zigmantas, D.; Hauer, J. Vibronic origin of long-lived coherence in an artificial molecular light harvester. *Nat. Commun.* **2015**, *6*, 7755.
(6) Collini, E. Cooperative effects to enhance two-photon absorption efficiency: intra- versus inter-molecular approach. *Phys. Chem. Chem. Phys.* **2012**, *14*, 3725.
(7) Kobayashi, T. *J-Aggregates*; World Scientific, 2012; Vol. *2*.
(8) Abramavicius, D.; Palmieri, B.; Voronine, D. V.; Šanda, F.; Mukamel, S. Coherent multidimensional optical spectroscopy of excitons in molecular aggregates; quasiparticle versus supermolecule perspectives. *Chem. Rev.* **2009**, *109*, 2350−2408.
(9) Davydov, A. S. The Theory of molecular excitons. *Sov. Phys. Usp.* **1964**, *7*, 145−178.
(10) May, V.; Kühn, O. Charge and Energy Transfer Dynamics in Molecular Systems. *Quantum* **2011**, 559−562.
(11) Van Amerongen, H.; Valkunas, L.; Van Grondelle, R. *Photosynthetic Excitons*; World Scientific, 2000.
(12) Scholes, G. D.; Rumbles, G. Excitons in nanoscale systems. *Nat. Mater.* **2006**, *5*, 683−696.
(13) Jumper, C. C.; Anna, J. M.; Stradomska, A.; Schins, J.; Myahkostupov, M.; Prusakova, V.; Oblinsky, D. G.; Castellano, F. N.; Knoester, J.; Scholes, G. D. Intramolecular radiationless transitions dominate exciton relaxation dynamics. *Chem. Phys. Lett.* **2014**, *599*, 23−33.
(14) Kassal, I.; Yuen-Zhou, J.; Rahimi-Keshari, S. Does coherence enhance transport in photosynthesis? *J. Phys. Chem. Lett.* **2013**, *4*, 362−367.
(15) Scholes, G. D.; Fleming, G. R.; Olaya-Castro, A.; van Grondelle, R. Lessons from nature about solar light harvesting. *Nat. Chem.* **2011**, *3*, 763−774.
(16) Fassioli, F.; Dinshaw, R.; Arpin, P. C.; Scholes, G. D. Photosynthetic light harvesting: excitons and coherence. *J. R. Soc., Interface* **2014**, *11*, 20130901.
(17) Cassette, E.; Pensack, R. D.; Mahler, B.; Scholes, G. D. Room-temperature exciton coherence and dephasing in two-dimensional nanostructures. *Nat. Commun.* **2015**, *6*, 6086.
(18) Myers, J. A.; Lewis, K. L. M.; Fuller, F. D.; Tekavec, P. F.; Yocum, C. F.; Ogilvie, J. P. Two-dimensional electronic spectroscopy of the D1-D2-cyt b559 photosystem II reaction center complex. *J. Phys. Chem. Lett.* **2010**, *1*, 2774−2780.
(19) Zigmantas, D.; Read, E. L.; Mančal, T.; Brixner, T.; Gardiner, A. T.; Cogdell, R. J.; Fleming, G. R.; et al. Two-dimensional electronic spectroscopy of the B800-B820 light-harvesting complex. *Proc. Natl. Acad. Sci. U. S. A.* **2006**, *103*, 12672−12677.
(20) Fidler, A. F.; Singh, V. P.; Long, P. D.; Dahlberg, P. D.; Engel, G. S. Time scales of coherent dynamics in the light-harvesting complex

DOI: 10.1021/acs.jpclett.6b02433
J. Phys. Chem. Lett. 2016, 7, 4996−5001

2 (LH2) of rhodobacter sphaeroides. *J. Phys. Chem. Lett.* **2013**, *4*, 1404−1409.
(21) Christensson, N.; Kauffmann, H. F.; Pullerits, T.; Mančal, T. Origin of long-lived coherences in light-harvesting complexes. *J. Phys. Chem. B* **2012**, *116*, 7449−7454.
(22) Tiwari, V.; Peters, W. K.; Jonas, D. M. Electronic resonance with anticorrelated pigment vibrations drives photosynthetic energy transfer outside the adiabatic framework. *Proc. Natl. Acad. Sci. U. S. A.* **2013**, *110*, 1203−8.
(23) Balaban, T. S. Tailoring Porphyrins and Chlorins for Self-Assembly in Biomimetic Artificial Antenna Systems. *Acc. Chem. Res.* **2005**, *38*, 612−613.
(24) Würthner, F.; Kaiser, T. E.; Saha-Möller, C. R. J-Aggregates: From Serendipitous Discovery to Supramolecular Engineering of Functional Dye Materials. *Angew. Chem., Int. Ed.* **2011**, *50*, 3376−3410.
(25) Ohno, O.; Kaizu, Y.; Kobayashi, H. J-aggregate formation of a water-soluble porphyrin in acidic aqueous media. *J. Chem. Phys.* **1993**, *99*, 4128.
(26) Micali, N.; Mallamace, F.; Romeo, A.; Purrello, R.; Monsù Scolaro, L. Mesoscopic Structure of meso -Tetrakis(4-sulfonatophenyl)porphine J-Aggregates. *J. Phys. Chem. B* **2000**, *104*, 5897−5904.
(27) Collini, E.; Ferrante, C.; Bozio, R. Strong enhancement of the two-photon absorption of tetrakis(4- sulfonatophenyl)porphyrin diacid in water upon aggregation. *J. Phys. Chem. B* **2005**, *109*, 2−5.
(28) Collini, E.; Ferrante, C.; Bozio, R. Influence of excitonic interactions on the transient absorption and two-photon absorption spectra of porphyrin J-asgregates in the NIR region. *J. Phys. Chem. C* **2007**, *111*, 18636−18645.
(29) Collini, E.; Ferrante, C.; Bozio, R.; Lodi, A.; Ponterini, G. Large third-order nonlinear optical response of porphyrin J-aggregates oriented in self-assembled thin films. *J. Mater. Chem.* **2006**, *16*, 1573.
(30) Occhiuto, I. G.; Zagami, R.; Trapani, M.; Bolzonello, L.; Romeo, A.; Castriciano, M. A.; Collini, E.; Monsù Scolaro, L. The role of counter-anions in the kinetics and chirality of porphyrin J-aggregates. *Chem. Commun.* **2016**, *52*, 11520−11523.
(31) Knoester, J.; Spano, F. C. *J-Aggregates*; World Scientific, 1996; p 111.
(32) Spano, F. C. Pump-probe spectrum of interacting one-dimensional excitons: biexcitons and J-aggregates. *Chem. Phys. Lett.* **1995**, *234*, 29−34.
(33) Chen, D.-M.; He, T.-J.; Cong, D.-F.; Zhang, Y.-H.; Liu, F.-C. Resonance Raman Spectra and Excited-State Structure of Aggregated Tetrakis(4-sulfonatophenyl)porphyrin Diacid. *J. Phys. Chem. A* **2001**, *105*, 3981−3988.
(34) Cho, M. *Two-Dimensional Optical Spectroscopy*; CRC Press, 2009; p 385.
(35) Bránczyk, A. M.; Turner, D. B.; Scholes, G. D. Crossing disciplines - A view on two-dimensional optical spectroscopy. *Ann. Phys.* **2014**, *526*, 31−49.
(36) Volpato, A.; Bolzonello, L.; Meneghin, E.; Collini, E. Global analysis of coherence and population dynamics in 2D electronic spectroscopy. *Opt. Express* **2016**, *24*, 24773.
(37) Tang, J.; Norris, J. R. Spectral analysis using linear prediction z-transform and autoregression. *Chem. Phys. Lett.* **1986**, *131*, 252−255.
(38) Caram, J. R.; Engel, G. S. Extracting dynamics of excitonic coherences in congested spectra of photosynthetic light harvesting antenna complexes. *Faraday Discuss.* **2011**, *153*, 93.
(39) Caram, J. R.; Lewis, N. H. C.; Fidler, A. F.; Engel, G. S. Signatures of correlated excitonic dynamics in two-dimensional spectroscopy of the Fenna-Matthew-Olson photosynthetic complex. *J. Chem. Phys.* **2012**, *136*, 104505.
(40) Nemeth, A.; Sperling, J.; Hauer, J.; Kauffmann, H. F.; Milota, F. Compact phase-stable design for single-and double-quantum two-dimensional electronic spectroscopy. *Opt. Lett.* **2009**, *34*, 3301−3303.
(41) Nemeth, A.; Milota, F.; Mancal, T.; Pullerits, T.; Sperling, J.; Hauer, J.; Kauffmann, H. F.; Christensson, N. Double-quantum two-dimensional electronic spectroscopy of a three-level system: Experiments and simulations. *J. Chem. Phys.* **2010**, *133*, 094505.
(42) Kim, J.; Mukamel, S.; Scholes, G. D. Two-Dimensional Electronic Double-Quantum Coherence Spectroscopy. *Acc. Chem. Res.* **2009**, *42*, 1375−1384.
(43) Stone, K. W.; Turner, D. B.; Gundogdu, K.; Cundiff, S. T.; Nelson, K. A. Exciton-exciton correlations revealed by twoquantum, two-dimensional fourier transform optical spectroscopy. *Acc. Chem. Res.* **2009**, *42*, 1452−1461.
(44) Knoester, J. Nonlinear optical susceptibilities of disordered aggregates: A comparison of schemes to account for intermolecular interactions. *Phys. Rev. A: At., Mol., Opt. Phys.* **1993**, *47*, 2083−2098.
(45) Spano, F. C. *J-Aggregates*; World Scientific, 2012; Vol. 2, Chapter 2, pp 64−69.
(46) Cheng, Y.-C.; Fleming, G. R. Coherence quantum beats in two-dimensional electronic spectroscopy. *J. Phys. Chem. A* **2008**, *112*, 4254−4260.
(47) Mukamel, S. *Principles of Nonlinear Optical Spectroscopy*; Oxford University Press, 1995.
(48) Fassioli, F.; Nazir, A.; Olaya-Castro, A. Quantum state tuning of energy transfer in a correlated environment. *J. Phys. Chem. Lett.* **2010**, *1*, 2139−2143.
(49) Brédas, J.-L.; Silbey, R. Excitons Surf Along Conjugated Polymer Chains. *Science* **2009**, *323*, 348−349.
(50) Fuller, F. D.; Pan, J.; Gelzinis, A.; Butkus, V.; Senlik, S. S.; Wilcox, D. E.; Yocum, C. F.; Valkunas, L.; Abramavicius, D.; Ogilvie, J. P. Vibronic coherence in oxygenic photosynthesis. *Nat. Chem.* **2014**, *6*, 706−11.
(51) Singh, V. P.; Westberg, M.; Wang, C.; Dahlberg, P. D.; Gellen, T.; Gardiner, A. T.; Cogdell, R. J.; Engel, G. S. Towards quantification of vibronic coupling in photosynthetic antenna complexes. *J. Chem. Phys.* **2015**, *142*, 212446.
(52) Malý, P.; Somsen, O. J. G.; Novoderezhkin, V. I.; Mančal, T.; Van Grondelle, R. The Role of Resonant Vibrations in Electronic Energy Transfer. *ChemPhysChem* **2016**, *17*, 1356−1368.
(53) Huo, P.; Coker, D. F. Influence of environment induced correlated fluctuations in electronic coupling on coherent excitation energy transfer dynamics in model photosynthetic systems. *J. Chem. Phys.* **2012**, *136*, 115102.

DOI: 10.1021/acs.jpclett.6b02433
J. Phys. Chem. Lett. 2016, 7, 4996−5001